Design of a SM-APID Control for Rigid-Body Transportation Under the Effects of Wind

Vincenzo Di Paola, Stéphane Caro, Matteo Zoppi

Design of a SM-APID Control for Rigid-Body Transportation Under the Effects of Wind

Vincenzo Di Paola, Stéphane Caro and Matteo Zoppi

University of Genova - DIME, Genova, Italy
vincenzo.dipaola@edu.unige.it, matteo.zoppi@unige.it
École Centrale de Nantes - LS2N, Nantes, France
stephane.caro@ls2n.fr

Abstract. Aerial transportation in windy conditions is challenging. In this paper, a pose-tracking task for a rigid body suspended by massless rigid bars and quadrotors, in presence of wind, is considered. To tackle the task, a Sliding Mode Adaptive Proportional-Integral-Derivative (SM-APID) control is designed. The proposed technique is tested through simulations and the performances are compared with a PID control.

Keywords: Aerial Systems, Load Transportation, Quadrotors, Sliding-Mode, Adaptive PID

Nomenclature

F_O, F_{Q_i}, F_G inertial frame, i^{th} drone frame and platform frame
$\mathbf{e}_1, \mathbf{e}_2, \mathbf{e}_3$ canonical base of inertial frame (O, x, y, z)
$m_i, m_L \in \mathbb{R}$ mass of the i^{th} drone and load, respectively
$\mathbf{R}_i, \mathbf{R}_o \in SO(3)$ orientation of the i^{th} robot/load with respect to F_O
$g \in \mathbb{R}$ gravity acceleration magnitude
$\boldsymbol{\Omega}_i, \dot{\boldsymbol{\Omega}}_i \in \mathbb{R}^3$ angular velocity, acceleration of the robot in F_{Q_i}
$\boldsymbol{\Omega}_o, \dot{\boldsymbol{\Omega}}_o \in \mathbb{R}^3$ angular velocity, acceleration of the platform in F_G
$f_i \in \mathbb{R}$ trust force of the i^{th} robot
$\mathbf{m}_i, \in \mathbb{R}^3$ control moment of the i^{th} robot in F_{Q_i}
$\mathbf{J}_i \in \mathbb{R}^{3\times3}$ inertia tensor of the i^{th} robot in F_{Q_i}
$\mathbf{m}_o, \in \mathbb{R}^3$ control moment of the i^{th} robot in F_{Q_i}
$\mathbf{J}_o \in \mathbb{R}^{3\times3}$ inertia tensor of the platform in F_G
$\mathbf{q}_i \in \mathbb{S}^2$ unit vector from the drone to the load in F_O
$\boldsymbol{\omega}_i \in \mathbb{R}^3$ angular velocity of the i^{th} link in F_O
$\mathbf{f}_{i,w}$, $\mathbf{f}_{L,w}, \mathbf{m}_{L,w}$ aerodynamic forces/moment acting on the system
$\mathbf{v}_i$ control force of the i^{th} robot
$\mathbf{v}_i^{\perp}, \mathbf{v}_i^{\parallel}$ orthogonal/parallel projection of $\mathbf{v}_i$ along $\mathbf{q}_i$
$\mathbf{x}_L$, position of frame F_G
$\mathbf{x}_L$, position of frame F_G
$\mathbf{k}_0, \mathbf{k}_1$ gain matrices
$\mathbf{r}_i$ attachment point on the platform w.r.t. F_G

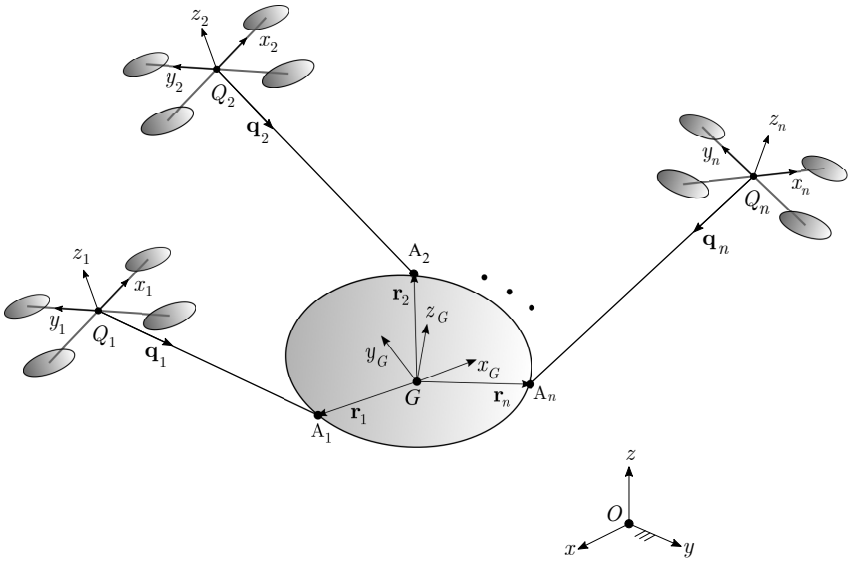

Fig. 1. Aerial System' Scheme: generic architecture of an aerial system with n quadrotors, rigid-bars and a rigid body platform.

1 Introduction

Over the past few years, the field of aerial transportation is attracting more and more attention from researchers. Indeed, the ability of drones to collaborate and accomplish various tasks has several practical applications [13, 16]. Among them, this paper focuses on rigid body transportation using a team of quadrotors and rigid links. For mentioned task, several control techniques are proposed in the literature, the most common range between flatness-based control [14] and geometric control [8, 1].

The direction taken by the current research is to make these systems as autonomous as possible. Indeed, in a recent paper [11] the authors tried to make the aerial system independent from the Motion Capture System (MOCAP) usually employed for controlling it whereas, in another work [4], the design of a new control strategy allowing facing wind gusts is introduced. These are indeed recent signs of steps toward outdoor and autonomous navigation.

With this in mind, the peculiarity of the task addressed here resembles into aerial transportation in presence of wind. Many wind models were developed so far. Among the existing ones, to reduce the computational cost while representing the main physical peculiarities of the wind, the Dryden model is used [3].

This work should be regarded as an extension of the previous work [4, 5] which considers a rigid body instead of a point of mass as a load. In other words, the Sliding-Mode Adaptive PID (SM-APID) control proposed is extended to guarantee tracking both the position and orientation of the platform while wind gusts are present.

This paper is structured as follows. Section 2 recalls the main equations governing the aerial system considered in this work. Section 3 describes the control technique used for this work. In section 4 a tracking task is assigned to the aerial system and the control performances in presence of wind and compared with a PID are shown. Finally, the results are summarized in Section 5.

2 System Modeling

Consider an aerial system with both n quadrotors and rigid links transporting a rigid body load along a given trajectory; as shown in Figure 1. In a similar fashion as in [4, 6, 15], by applying Hamilton's principle and rearranging the equations, one gets the equations of motion for the entire system

$$
\begin{cases}
\dfrac{d}{dt}\mathbf{x}_L = \dot{\mathbf{x}}_L, & (1)\\
\Big(\displaystyle\sum_{i=1}^{n} m_i\mathbf{q}_i\mathbf{q}_i^T + m_L\mathbf{I}\Big)(\ddot{\mathbf{x}}_L + g\mathbf{e}_3) - \displaystyle\sum_{i=1}^{n} m_i\mathbf{q}_i\mathbf{q}_i^T\mathbf{R}_o\tilde{\mathbf{r}}_i\dot{\boldsymbol{\Omega}}_o = & \\
\qquad \displaystyle\sum_{i=1}^{n}\big(\mathbf{v}_i^{\parallel} - m_i l_i||\boldsymbol{\omega}_i||^2\mathbf{q}_i + (\mathbf{q}_i\cdot\mathbf{f}_{i,w})\mathbf{q}_i - m_i\mathbf{q}_i\mathbf{q}_i^T\mathbf{R}_o\tilde{\boldsymbol{\Omega}}_o^2\mathbf{r}_i\big) + \mathbf{f}_{L,w}, & (2)\\
\dot{\mathbf{q}}_i = \boldsymbol{\omega}_i\times\mathbf{q}_i, & (3)\\
\dot{\boldsymbol{\omega}}_i = \dfrac{1}{l_i}\hat{\mathbf{q}}_i(\ddot{\mathbf{x}}_L + g\mathbf{e}_3 - \mathbf{R}_o\tilde{\mathbf{r}}_i\dot{\boldsymbol{\Omega}}_o - \mathbf{R}_o\tilde{\boldsymbol{\Omega}}_o^2\mathbf{r}_i) - \dfrac{1}{m_i l_i}\hat{\mathbf{q}}_i\mathbf{v}_i^{\perp} - \dfrac{1}{m_i l_i}\hat{\mathbf{q}}_i\mathbf{f}_{i,w}, & (4)\\
\dot{\mathbf{R}}_i = \mathbf{R}_i\hat{\boldsymbol{\Omega}}_i, & (5)\\
\mathbf{m}_i = \mathbf{J}_i\dot{\boldsymbol{\Omega}}_i + \boldsymbol{\Omega}_i\times\mathbf{J}_i\boldsymbol{\Omega}_i, \dot{\mathbf{R}}_o = \mathbf{R}_o\hat{\boldsymbol{\Omega}}_o, & (6)\\
\mathbf{m}_o = \mathbf{J}_o\dot{\boldsymbol{\Omega}}_o + \boldsymbol{\Omega}_o\times\mathbf{J}_o\boldsymbol{\Omega}_o - \mathbf{m}_{L,w}, & (7)
\end{cases}
$$

where $\mathbf{I}$ identifies the identity matrix of dimension three.

3 Sliding-Mode Adaptive PID

The objective of the control is to ensure that the platform tracks the desired pose under the action of external disturbances.
Generally, the Sliding Mode (SM) control is used to guide a system under the effect of disturbances and uncertainties. To avoid typical chattering of the SM control, the main control command is demanded to an Adaptive PID which is added to the SM part. The fusion of the two will enable controlling the systems in presence of external disturbances limiting the chattering issue.

3.1 Control Structure

The control input is split into two terms [7, 18]

$$\mathbf{u} = \mathbf{u}_{PID} + \mathbf{u}_s, \tag{8}$$

where $\mathbf{u}_s$ is the supervisory control that keeps the system state within some defined boundaries guaranteeing the stability of the dynamical system. The PID exploits a gradient-based adaptation law for updating its gains providing robustness of the control. The design of both $\mathbf{u}_s$ and $\mathbf{u}_{PID}$ has been defined in [2].

3.2 Design of the Supervisory Control

The role of $\mathbf{u}_s$ is to keep the system state inside a designed constraint set

$$\mathfrak{C} = \{\mathbf{x} \in \mathbb{R}^{2n} | \, ||\mathbf{x}|| \leq M_{\mathbf{x}}\}, \tag{9}$$

where $\mathbf{x} = \left[\tilde{\mathbf{x}}, \dot{\tilde{\mathbf{x}}}\right]^T$ is the system' state vector while $M_{\mathbf{x}}$ is a pre-specified parameter usually chosen such that $M_{\mathbf{x}} \geq \ ||\mathbf{y}||_\infty$ with $\mathbf{y}$ representing the desired state vector.

Its design relies on the stability of the system. Hence, to asymptotically attain the zero-error condition, the following Lyapunov function candidate is considered

$$V_e = \frac{1}{2}\mathbf{e}^T \mathbf{\Phi} \mathbf{e}, \tag{10}$$

where $\mathbf{e} = \left[\tilde{\mathbf{e}}, \dot{\tilde{\mathbf{e}}}\right]^T \in \mathbb{R}^{2n}$ and $\dot{\mathbf{e}} = \left[\dot{\tilde{\mathbf{e}}}, \ddot{\tilde{\mathbf{e}}}\right]^T \in \mathbb{R}^{2n}$ are the state error vectors and its derivative with $\ddot{\tilde{\mathbf{e}}}$ and $\dot{\tilde{\mathbf{e}}}$ time derivatives of $\tilde{\mathbf{e}} = \mathbf{y} - \mathbf{x}$. Generally, $\mathbf{\Phi}$ is defined as a positive definite and symmetric matrix that springs out as the solution of the Lyapunov equation [19, 2]

$$\mathbf{A}^T \mathbf{\Phi} + \mathbf{\Phi} \mathbf{A} = -\mathbf{Q}, \tag{11}$$

where matrix $\mathbf{Q} \in \mathbb{R}^{2n \times 2n}$ is a given, positive definite symmetric matrix whereas matrix $\mathbf{A} \in \mathbb{R}^{2n \times 2n}$ pops out by rewriting the error dynamic.

A classical strategy to reach the desired output is to exercise a control action that strictly decreases V_e, which means that $\mathbf{u}_s$ must meet

$$\dot{V}_e < 0. \tag{12}$$

The derivative of the Lyapunov function can be computed as follows

$$\dot{V}_e = \frac{1}{2}(\dot{\mathbf{e}}^T \mathbf{\Phi} \mathbf{e} + \mathbf{e}^T \mathbf{\Phi} \dot{\mathbf{e}}) \leq -\frac{1}{2}\mathbf{e}^T \mathbf{Q} \mathbf{e} + |\mathbf{e}^T \mathbf{\Phi} \mathbf{B}|(|\mathbf{u}^*| + |\mathbf{u}_{PID}|) - \mathbf{e}^T \mathbf{\Phi} \mathbf{B} \mathbf{u}_s. \tag{13}$$

Therefore, to satisfy Eq.(13), the supervisory controller can be chosen as

$$\mathbf{u}_s = \text{sgn}(\mathbf{e}^T \mathbf{\Phi} \mathbf{B}(|\mathbf{u}^*| + |\mathbf{u}_{PID}|). \tag{14}$$

With this design, $\mathbf{u}_s$ constantly intervenes in the control process and the presence of sgn function leads to chattering. Therefore, to adhere with its supervisory definition and to reduce the chattering the set of constraints $\mathfrak{C}$ is used. In particular, the Indicator function I_f is introduced in the $\mathbf{u}_s$ design as follows

$$\tilde{\mathbf{u}}_s = I_f \, \mathbf{u}_s, \quad \text{where} \quad I_f = \begin{cases} 1, & V_e > V_M, \\ 0, & V_e \leq V_M, \end{cases} \tag{15}$$

with

$$V_M = \frac{1}{2}\lambda_{min}(\mathbf{\Phi})(M_{\mathbf{x}} - ||\mathbf{y}||_\infty)^2, \tag{16}$$

where $\lambda_{min}(\mathbf{\Phi})$ is the minimum eigenvalue of the Lyapunov matrix $\mathbf{\Phi}$ [2, 19]. The introduction of the Indicator function completes its design.

3.3 PID Adaptive Laws

The APID is then supposed to steer the system under ordinary conditions (i.e. $V_e \leq V_M$). The adaptation laws are derived with the aim to reach the so-called sliding mode $\mathcal{S} = \mathbf{0}$ (i.e. insensitivity to external disturbances) where $\mathcal{S}$ is the sliding surface defined as [18]

$$\mathcal{S} = \dot{\mathbf{x}} - \mathbf{x}_r = \dot{\mathbf{x}} - \dot{\mathbf{y}} - \mathbf{k}_1\tilde{\mathbf{e}} - \mathbf{k}_0 \int \tilde{\mathbf{e}}\, dt, \tag{17}$$

where $\mathbf{x}_r$ is the so-called reference signal. To guarantee approaching the sliding mode the Lyapunov function approach is exploited with a Lyapunov function candidate as

$$V = \frac{1}{2}\mathcal{S}^2. \tag{18}$$

Again, requiring that $\mathcal{S}(t) \to \mathbf{0}$ for $t \to \infty$ coincide with reducing V. Consequently, the gradient method is employed to choose the gains which take directions of maximum slope over V. Now, the common expression for a PID controller is

$$\mathbf{u}_{PID} = \mathbf{K}_P\tilde{\mathbf{e}} + \mathbf{K}_I \int \tilde{\mathbf{e}}\, dt + \mathbf{K}_D\dot{\tilde{\mathbf{e}}}, \tag{19}$$

using the gradient method and the chain rule, it is possible to obtain the adaptation laws for the control gain matrices $\mathbf{K}_P$, $\mathbf{K}_I$ and $\mathbf{K}_D$

$$\dot{\mathbf{K}}_{P,ii} = -\gamma\frac{\partial\mathcal{S}\dot{\mathcal{S}}}{\partial\mathbf{K}_P} = -\gamma\frac{\partial\mathcal{S}\dot{\mathcal{S}}}{\partial\mathbf{u}_{PID}}\frac{\partial\mathbf{u}_{PID}}{\partial\mathbf{K}_P} = -\gamma\mathcal{S}\tilde{\mathbf{e}}, \tag{20a}$$

$$\dot{\mathbf{K}}_{I,ii} = -\gamma\frac{\partial\mathcal{S}\dot{\mathcal{S}}}{\partial\mathbf{K}_I} = -\gamma\frac{\partial\mathcal{S}\dot{\mathcal{S}}}{\partial\mathbf{u}_{PID}}\frac{\partial\mathbf{u}_{PID}}{\partial\mathbf{K}_I} = -\gamma\mathcal{S}\int \tilde{\mathbf{e}}\, dt, \tag{20b}$$

$$\dot{\mathbf{K}}_{D,ii} = -\gamma\frac{\partial\mathcal{S}\dot{\mathcal{S}}}{\partial\mathbf{K}_D} = -\gamma\frac{\partial\mathcal{S}\dot{\mathcal{S}}}{\partial\mathbf{u}_{PID}}\frac{\partial\mathbf{u}_{PID}}{\partial\mathbf{K}_D} = -\gamma\mathcal{S}\dot{\tilde{\mathbf{e}}}, \tag{20c}$$

where minus is placed opposite to the energy flow V and $\gamma \in \mathbb{R}^+$ is called learning rate[1].

Hence, the behaviour of the controller can be resumed as follows: if $\mathbf{u}_s = \mathbf{0}$, the PID gains adapt themselves to decrease V to zero (i.e. reach the sliding mode) whereas if $\mathbf{u}_s \neq \mathbf{0}$, the PID gains are not able to decrease V and then also V_e under V_M.

[1] To avoid cumbersome notation, the subscripts ii (emphasizing the diagonal structure of the gain matrices) have been inserted only on the left-hand side of the equation, intending the derivative operation to be carried out component-wise, as is typical in the literature [12].

3.4 Design of the Parallel Components

The parallel component is chosen to track the desired pose $\mathbf{p}^{des} = (\mathbf{x}_L^{des}, \mathbf{R}_o^{des})$ of the load, in other words it is necessary to define $\mathbf{v}_i^{\parallel}$ s.t. $\mathbf{p} \longrightarrow \mathbf{p}^{des}$ while $t \longrightarrow \infty$.

Consider the load Equation (2). Then, it is possible to derive $\mathbf{v}_i^{\parallel}$ as

$$\mathbf{v}_i^{\parallel} = m_i l_i ||\boldsymbol{\omega}_i||^2 \mathbf{q}_i + t_i \mathbf{q}_i + m_i \mathbf{q}_i \mathbf{q}_i^T (\ddot{\mathbf{x}}_L + g\mathbf{e}_3 + \mathbf{R}_o \tilde{\boldsymbol{\Omega}}_o^2 \rho_i - \mathbf{R}_o \tilde{\boldsymbol{\rho}}_i \dot{\boldsymbol{\Omega}}_o) - (\mathbf{q}_i \cdot \mathbf{f}_{i,w}) \mathbf{q}_i, \tag{21}$$

where t_i represent the tension along the i^{th} link. To find the tensions to be applied along the links, it is enough to refer to the platform dynamics described as

$$\mathbf{W}\mathbf{t} + \mathbf{w}_e = \mathbf{0} \quad \text{where} \quad \mathbf{W} = \begin{bmatrix} \mathbf{q}_1 & \mathbf{q}_2 & \cdots & \mathbf{q}_n \\ \tilde{\mathbf{r}}_1 \mathbf{q}_1 & \tilde{\mathbf{r}}_2 \mathbf{q}_2 & \cdots & \tilde{\mathbf{r}}_n \mathbf{q}_n \end{bmatrix}, \tag{22}$$

is the so-called wrench matrix whereas $\mathbf{t}$ is the vector of the tensions components along the rigid-bars and $\mathbf{w}_e$ is the external wrench vector containing all the external forces, moments and inertial terms. A common solution to Eq. (22) relies on the use of the pseudo-inverse

$$\mathbf{t} = -\mathbf{W}^{\dagger} \mathbf{w}_e, \tag{23}$$

where $\mathbf{W}^{\dagger} = \mathbf{W}^T (\mathbf{W}\mathbf{W}^T)^{-1}$ is the $\mathbf{W}$ pseudo-inverse.
Observe that $\mathbf{w}_e$ takes the role of the control actions $\mathbf{u}_f$ and $\mathbf{u}_m$ therefore, Eq.(23) becomes

$$\mathbf{t} = -\operatorname{diag}(\mathbf{R}_o) \mathbf{W}^{\dagger} \begin{bmatrix} \mathbf{R}_o^T \mathbf{u}_f \\ \mathbf{u}_m \end{bmatrix}, \tag{24}$$

where $\mathbf{w}^{des} = [\mathbf{R}_o^T \mathbf{u}_f, \, \mathbf{u}_m]^T$ which represents the action necessary to compensate for the external forces, disturbances and then correct the tracking error.

3.5 Design of the Orthogonal Components

The normal component is chosen to reach the desired configuration of the system [1, 17], in other words it becomes necessary to define $\mathbf{v}_i^{\perp}$ s.t. $\mathbf{q}_i \longrightarrow \mathbf{q}_i^{des}$ while $t \longrightarrow \infty$. In particular, the direction and angular velocity errors, are defined as follows

$$\mathbf{e}_{\mathbf{q}_i} = \mathbf{q}_i^{des} \times \mathbf{q}_i \quad \text{and} \quad \mathbf{e}_{\boldsymbol{\omega}_i} = \boldsymbol{\omega}_i + \hat{\mathbf{q}}_i^2 \boldsymbol{\omega}_i^{des}, \tag{25}$$

whereas, the desired angular acceleration is

$$\dot{\boldsymbol{\omega}}_i = -K_{\mathbf{q}_i} \mathbf{e}_{\mathbf{q}_i} - K_{\boldsymbol{\omega}_i} \mathbf{e}_{\boldsymbol{\omega}_i} - (\mathbf{q}_i \cdot \boldsymbol{\omega}_i^{des}) \dot{\mathbf{q}}_i - \hat{\mathbf{q}}_i^2 \dot{\boldsymbol{\omega}}_i^{des}, \tag{26}$$

for positive gains $K_{\mathbf{q}_i}$ and $K_{\boldsymbol{\omega}_i}$. Now, rearranging equations of motion and using Eq.(26) yields to the expression for the normal component $\mathbf{v}_i^{\perp}$ [10]

$$\mathbf{v}_i^{\perp} = m_L l_i \hat{\mathbf{q}}_i (-K_{\mathbf{q}_i} \mathbf{e}_{\mathbf{q}_i} - K_{\boldsymbol{\omega}_i} \mathbf{e}_{\boldsymbol{\omega}_i} - (\mathbf{q}_i \cdot \boldsymbol{\omega}_i^{des}) \dot{\mathbf{q}}_i - \hat{\mathbf{q}}_i^2 \dot{\boldsymbol{\omega}}_i^{des}) - \frac{m_i}{m_L} \hat{\mathbf{q}}_i^2 \sum_{j=1,\, j \neq i}^{n} t_j \mathbf{q}_j + \hat{\mathbf{q}}_i^2 \mathbf{f}_{i,w}. \tag{27}$$

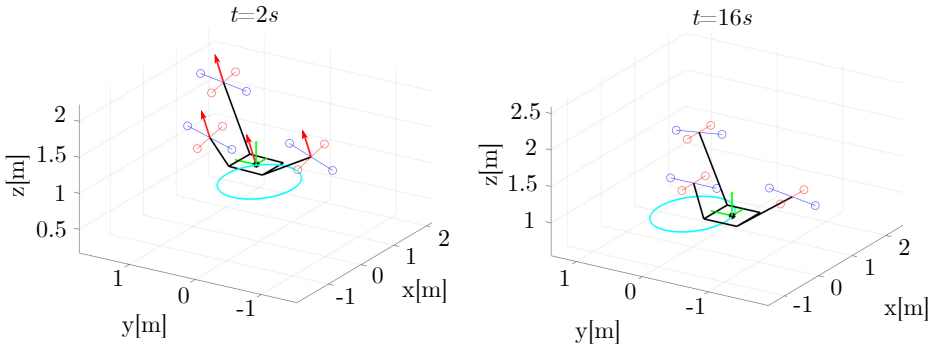

Fig. 2. Simulation: two phases of the simulation with the SM-APID control are depicted. One at the time $t = 2\,s$ where the wind, depicted as red arrows, is acting on the quadrotors and platform whereas, in the second image, one sees the attitude of the system when the wind is not present anymore namely at $t = 16\,s$.

3.6 Quadrotor's Attitude Control

To fully control the overall system, the attitude control of each quadrotor must be included. However, due to space limitations, the equations are not reported as they are well known in the literature; the reader is referred to [4, 9].

4 Study Case

In this section, an aerial system with three quadrotors and rigid-bars is considered. The aim consists in tracking an elliptical trajectory while orienting the platform in presence of wind. Hence, Figure 2 is intended to give an idea of the task the system has to fulfil and how it behaves in the presence and absence of wind. As a general comment, it is evident how, in presence of the wind, the drones' attitude is such that they resist it. In fact, their orientation is completely different when the wind disappears. Furthermore, because of wind, tracking errors are expected to be affected by greater variations (wider oscillations of the profiles) since wind changes direction continuously.

Regarding the simulation data, the mass of the platform is $m_L = 0.5\,kg$, its length, width and height are $0.7\,m$, $0.5\,m$ and $0.2\,m$, respectively while its inertia matrix is $\mathbf{J}_o = \text{diag}(0.15, 0.15, 0.17)\,kg\,m^2$. Bar lengths are $l_i = 1m$ (massless). Quadrotors' masses are $m_i = 1.15kg$ while $\mathbf{J}_i = \text{diag}(0.1, 0.1, 0.14)kg\,m^2$. The attachment points on the platform are $\mathbf{d}_1 = [-0.35, -0.25, 0]\,m$, $\mathbf{d}_2 = [-0.35, 0.25, 0]\,m$ and $\mathbf{d}_3 = [0.35, 0.25, 0]\,m$. The initial conditions, necessary to replicate the results are $\mathbf{x}_L(0) = [0.75, 0, 0.5]$, $\boldsymbol{\Omega}_i(0) = \boldsymbol{\Omega}_o(0) = \dot{\mathbf{x}}_L(0) = \boldsymbol{\omega}_i(0) = [0, 0, 0]$ while the bar directions are $\mathbf{q}_1(0) = [\sin 60, 0, -\cos 60]$, $\mathbf{q}_2(0) = [0, -\sin 60, -\cos 60]$ and $\mathbf{q}_3(0) = [-\sin 60, 0, -\cos 60]$ whereas $\mathbf{R}_o(0) = -\mathbf{I}$ and $\mathbf{R}_o^{des} = \mathbf{I}$. Wind actions on the system are generated by using the Dryden model, in analogy with the works [3, 4]. Here, the maximum wind velocities are 6m/s

along the x-y plane and 2m/s along the z direction, respectively. The forces and moments acting on the objects depend on their shapes.

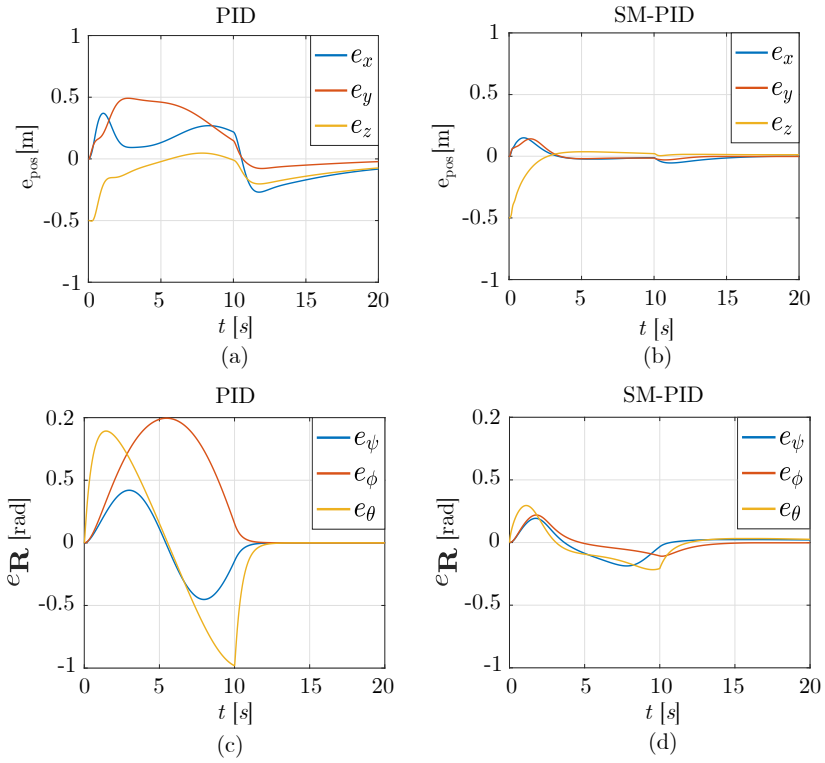

Fig. 3. Pose Errors: a comparisons between the position (a)-(b) and orientation (c)-(d) errors of the platform using the PID and SM-APID control. Observe that angles ψ, ϕ and θ represent the yaw, pitch and roll angles of the platform respectively.

The entire simulation lasts $20s$ and in the middle of the simulation, the wind is suddenly removed to see the behaviour of the control and the reaction of the system. This should simulate the appearance and disappearance of the wind as experienced in practice.

Since the task resembles in tracking the desired pose, the interest in the simulation results, for the proposed SM-APID and PID controls, lies in the tracking pose errors reported in Fig.3.

Firstly, it is evident that the errors for both the position and orientation are always smaller in the case of the SM-APID control. This is then a clear evidence of the superior robustness of the proposed method w.r.t. the classical PID commonly used.

Secondly, from the PID graphs (a)-(c) one can see that, when the wind disappears at $t = 10s$ onward, the PID recover as much as possible the accumulated

error on both sides, i.e., position and orientation. However, even if the error is reduced, the system undertakes a sudden manoeuvre that can be considered unsafe for certain types of tasks. This behaviour is not so pronounced in the case of SM-APID. Indeed, when the wind disappears, the gains stabilize and the errors tend to 0.

Finally, it is worth remembering that to achieve *acceptable* performances with a PID, the gains must be tuned iteratively. Thus, the ability to adjust gains automatically turns out to be an effective strategy that combines robustness and practicality. However, it should be pointed out that, as stated in Sec.3.3, if the external disturbance is not sufficiently bounded, gain adaptation may not be prompt enough. In that case, the typical sliding mode would be activated guaranteeing the desired robustness at the price of introducing chattering.

5 Conclusion

In this paper, the design of the SM-APID was presented for an aerial system transporting a rigid body in presence of wind. The proposed control is guaranteed to asymptotically follow the desired pose in presence of bounded disturbances. Its performances were compared with the well-known PID control. The obtained results not only confirmed the superiority of SM-APID over PID but provide further motivation to invest in hardware allowing testing this technique through experimental validation.

References

1. Bullo, F., Lewis, A.D.: Geometric control of mechanical systems: modeling, analysis, and design for simple mechanical control systems. Springer, Texts in Applied Mathematics (2005). https://doi.org/10.1007/978-1-4899-7276-7
2. Chang, W.D., Yan, J.J.: Adaptive robust pid controller design based on a sliding mode for uncertain chaotic systems. Chaos, Solitons & Fractals (2005). https://doi.org/https://doi.org/10.1016/j.chaos.2004.12.013
3. Cole, K., Wickenheiser, A.: Spatio-temporal wind modeling for uav simulations. arXiv (2019). https://doi.org/arXiv:1905.09954
4. Di Paola, V., Goldsztejn, A., Zoppi, M., Caro, S.: Design of a sliding mode-adaptive proportional-integral-derivative control for aerial systems with a suspended load exposed to wind gusts. Journal of Computational and Nonlinear Dynamics (2023). https://doi.org/doi.org/10.1115/1.4062324
5. Di Paola, V., Ida', E., Zoppi, M., Caro, S.: A preliminary study of factors influencing the stiffness of aerial cable towed systems. ROMANSY, Springer International Publishing (2022). https://doi.org/10.1007/978-3-031-06409-8-29
6. Di Paola, V.: Contributions to open problems on cable driven robots and persistent manifolds for the synthesis of mechanisms. University of Genova and Ecole Centrale de Nantes, Doctoral Thesis (2023). https://doi.org/https://hdl.handle.net/11567/1153244
7. Hsueh, Y.C., Su, S.F.: Supervisory controller design based on lyapunov stable theory. 2007 IEEE International Conference on Systems, Man and Cybernetics (2007). https://doi.org/10.1109/ICSMC.2007.4413948

8. Lee, T.: Geometric control of quadrotor uavs transporting a cable-suspended rigid body. IEEE Transactions on Control Systems Technology (2014). https://doi.org/10.1109/TCST.2017.2656060
9. Lee, T., Leok, M., McClamroch, N.: Geometric tracking control of a quadrotor uav on se(3). Proceedings of the IEEE Conference on Decision and Control (2010). https://doi.org/10.1109/CDC.2010.5717652
10. Lee, T., Sreenath, K., Kumar, V.: Geometric control of cooperating multiple quadrotor uavs with a suspended payload. 52nd IEEE Conference on Decision and Control (2013). https://doi.org/10.1109/CDC.2013.6760757
11. Li, Z., Erskine, J., Caro, S., Chriette, A.: Design and control of a variable aerial cable towed system. IEEE Robotics and Automation Letters (2020). https://doi.org/10.1109/LRA.2020.2964165
12. Noordin, A., Mohd Basri, M.A., Mohamed, Z., Mat Lazim, I.: Adaptive pid controller using sliding mode control approaches for quadrotor uav attitude and position stabilization. Arabian Journal for Science and Engineering (2021). https://doi.org/10.1007/s13369-020-04742-w
13. Ollero, A., Siciliano, B.: Aerial Robotic Manipulation. Springer Tracts in Advanced Robotics (2019). https://doi.org/https://doi.org/10.1007/978-3-030-12945-3
14. Sreenath, K., Kumar, V.: Dynamics, control and planning for cooperative manipulation of payloads suspended by cables from multiple quadrotor robots. Robotics: Science and Systems IX (2013). https://doi.org/10.15607/RSS.2013.IX.011
15. Taeyoung Lee, Melvin Leok, N.H.M.: Global Formulations of Lagrangian and Hamiltonian Dynamics on Manifolds: A Geometric Approach to Modeling and Analysis. Springer International Publishing (2017). https://doi.org/https://doi.org/10.1007/978-3-319-56953-6
16. Tognon, M., Franchi, A.: Theory and Applications for Control of Aerial Robots in Physical Interaction Through Tethers. Springer Tracts in Advanced Robotics (2020). https://doi.org/https://doi.org/10.1007/978-3-030-48659-4
17. Wu, G., Sreenath, K.: Variation-based linearization of nonlinear systems evolving on $so(3)$ and $\mathbb{S}^2$. IEEE Access (2015). https://doi.org/10.1109/ACCESS.2015.2477880
18. Yuri, S., Christopher, E., Leonid, F., Arie, L.: Sliding Mode Control and Observation. Birkhäuser, New York, NY (2014). https://doi.org/https://doi.org/10.1007/978-0-8176-4893-0
19. Zabczyk, J.: Mathematical Control Theory, An Introduction. Birkhäuser, Cham (2020). https://doi.org/https://doi.org/10.1007/978-3-030-44778-6